Microstructural origin of switching field distribution in patterned Co/Pd multilayer nanodots

J. W. Lau* and R. D. McMichael
Metallurgy Division, National Institute of Standards and Technology, Gaithersburg, MD 20899

S. H. Chung
Center for Nanoscale Science and Technology, National Institute of Standards and Technology, Gaithersburg, MD 20899 and Maryland NanoCenter, University of Maryland, College Park, MD 20742

J. O. Rantschler, V. Parekh, and D. Litvinov
Center for Nanomagnetic Systems, University of Houston, Houston, TX 77204

(Dated: April 4, 2008)

We have identified an important origin of the switching field distribution (SFD) in patterned Co/Pd multilayer nanodots. In this study, a marked array of 115 nm Co/Pd nanodots on 50-nm thick Si_3N_4 substrate. We identified the dots with unusually small and large (>2 standard deviations of the mean) switching fields with magnetic force microscopy, followed by microstructural characterization of the same dots with transmission electron microscopy (TEM). From electron diffraction, we found that most nanodots with small switching fields have strong (200) spots, whereas those with large switching fields lack these spots. While bright-field TEM images reveal an average grain size of 7 nm, dark-field images of the (200) spots reveal on average, a single grain of >10 nm in lateral dimensions. Since we observed a direct correlation between strong (200) reflections and small reversal fields, we conclude that the largest grain in each nanodot with an in-plane [001] is the likely cause for premature switching, which in turn defines the SFD of this array.

PACS numbers: 75.75.+a, 81.07.b
Keywords: switching field distribution, microstructure, grain orientation

Patterned media is a promising candidate for replacing continuous film media for ultra-high density (>1 Tb/in^2) magnetic recording[1–5]. In particular, the Co/Pd multilayer system is of interest due to its perpendicular anisotropy[4,6–8] and tunable intergranular coupling[9]. In order to make patterned media technologically viable, the industry must overcome an important obstacle, that is, ensuring that all of the bits in the media switch at the same field, i.e., reducing the SFD. There are many causes for SFD; e.g., thermal effects[10,11], edge roughness[12,13], edge oxidation[14] and choice of seed-layers[9,15,16]. Interactions with neighboring dots have also been shown to increase SFD[17]; such contributions have been measured experimentally[18].

Previous work by Thomson et. al indicated that inter-element variations due to the fabrication process contribute minimally to the SFD in Co/Pd multilayers[19]. Without identifying a specific microstructural origin, the authors showed that the dot-size dependence of the SFD is consistent with sampling a distribution of nucleation volumes[19]. Since the Co/Pd nanodots are polycrystalline, this "nucleation volume" may originate from certain grain(s) within each nanodot. We therefore focus on microstructure as the origin of SFD in this work. The lay-out of the experiment is as follows: first, we identify individual dots within the Co/Pd patterned array that are particularly "easy" (requires small) or "stubborn" (requires large reversal field) to switch. Next, we record the locations of the easy and stubborn switchers within the array. Lastly, we conduct a diffraction study on each abberent nanodot and note any differences in crystalline quality between the nanodots at the two ends of the SFD.

Co/Pd multilayers (Ta 2.5 /Pd 5/[Co 0.3 /Pd 0.35]$_{10}$/Ta 1 nm) were deposited by dc magnetron sputtering onto a 50-nm thick Si_3N_4 membrane window. The first two layers in the stack encouraged the growth of fcc cobalt in the subsequent layers; the final layer served as an oxidation barrier. The pattern was written by electron-beam lithography on poly-methyl methacrylate resist and development in 3:1::isopropanol:methyl isobutyl ketone. Next, 20-nm thick Al mask was thermally evaporated onto the film and then lifted off. An Ar sputter etch removed the region of magnetic multilayers not protected by Al. Lastly, residual Al was removed. The final product was a $50 \times 50\mu$m indexed array, where the diameter of the nanodots and the pitch was 115 and 223 ± 6 nm, respectively. However, in order to optimize resolution and statistics for both the magnetic force microscopy (MFM) and TEM analysis, our region of interest is confined to a $20 \times 20\mu$m area, or ∼3600 dots.

We applied magnetic fields normal to the film plane with a pair of NdFeB magnets set in a steel vise. Since the diameter of the magnets are 3 orders of magnitude larger than the area of interest on the sample, we consider the field across the sample to be uniform. We changed

the field applied to the sample by adjusting the gap between the two magnets which were calibrated with a Hall probe. From our MFM observations, we found that a 4 mm gap saturated the entire array. The array was re-saturated each time before a reverse field was applied. We analyzed in detail, MFM images of the patterned array recorded at two reversed-field values, 279 and 573 kA/m, that switched 2 and 99% of the dots respectively. We identified the population of dots with switching field <279 kA/m as easy switchers; dots with switching fields >573 kA/m are the stubborn switchers. The coordinates of every easy and stubborn switcher were recorded so that the same dots may be re-identified once the sample is transfered to the TEM.

Knowing the locations of the easy and stubborn switchers, we looked for differences in their microstructure in the TEM. Physical quality of the dots was accessed with bright field images, while more in depth microstructural information was obtained from selected-area electron diffraction pattern of the individual dots. If a diffraction pattern contained interesting features, an objective aperture was inserted to isolate these features for dark-field imaging.

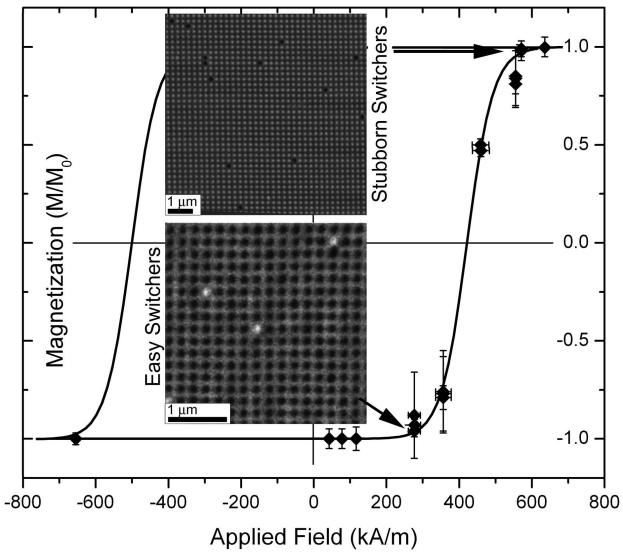

FIG. 1: Hysteresis loop based on MFM data. When saturated, each dot within the array appears black. As we apply the reversed field, the dots begin to switch and appear white. Arrows indicate the part of the loop where the MFM images were taken.

The hysteresis loop in fig. 1 was obtained by fitting our MFM data with an error function. From the fit, we obtained 425 kA/m as the coercivity and 58 kA/m as the 1σ value of the SFD. The uncertainty in M/M_0 was calculated from the statistics of N dots in a given image ($\propto 1/\sqrt{N}$). The uncertainty in the applied field was experimentally measured. The MFM images in fig. 1, labeled easy and stubborn switchers, were acquired at 279 and 573 kA/m, respectively. The easy switchers appear as white dots whereas the stubborn switchers appear as black dots. In all, 36 easy switchers and 25 stubborn switchers were identified for further TEM analysis.

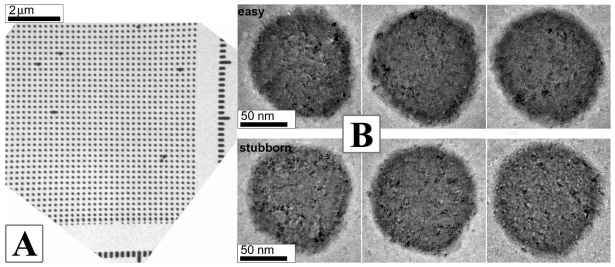

FIG. 2: (a) TEM image of the patterned array. (b) Bright-field images of nanodots requiring small switching fields (top) and large switching fields (bottom). The two sets are nominally indistinguishable

Except the dots at the edge of the array, all dots including those with exceptionally high and low switching fields, appeared nominally identical as seen in [fig. 2a]. From bright-field TEM images, there were no discernable difference between the easy and stubborn switchers, that is, both sets had randomly oriented grains with similar sizes and shapes. The shape of the dots and their edge characteristics did not differ appreciably between the two sets.

Electron diffraction on individual dots revealed the underlying microstructural causes of the disparity in switching fields. For these measurements, the electron beam illuminated the entire dot. Using Au as a calibration standard, we measured[20] the interplanar spacing giving rise to the first four Debye rings in our Co/Pd dots,(111), (200), (220), and (311) as 0.229 ± 0.002, 0.205 ± 0.001, 0.136 ± 0.001, 0.118 ± 0.001 nm, respectively. We found no appreciable differences in ring radii between the easy and the stubborn dots.

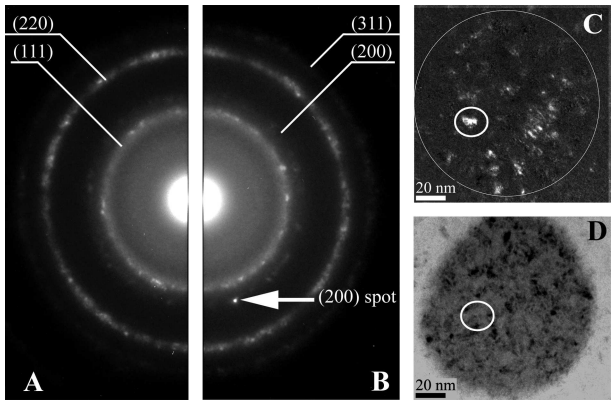

FIG. 3: (a) plan-view diffraction pattern of a Co/Pd nanodot with large switching field (stubborn switcher). (b) diffraction pattern of nanodot with small switching field (easy switcher). (c) a dark-field TEM image; the circled grain is responsible for the (200) spot observed in (b). (d) bright-field image of the same nanodot given in (b) and (c). The circled region corresponds to the reflecting crystal in (c).

We found differences between the easy and stubborn switchers in the (200) reflections. Among the stubborn switchers (fig. 3a), the (200) rings had near-uniform intensities in all directions within the specimen plane; this is consistent with a polycrystalline sample where each dot is comprised of hundreds of randomly-oriented grains. In the easy switchers however, many (78%) exhibit at least one pair of high-intensity (200) spots along the ring (fig. 3b, shows one of the spot pairs. The second spot of the pair is located at the other half of fig. 3b, not shown). For the remaining easy-switchers with missing (200) reflections, if the 200-Bragg condition is in close proximity, then a small tilt should reveal the (200) spots. We tilted the sample $\leq 2^\circ$ and found that 94% of the easy switchers now produced sharp (200) spots.

In order to compare the (200) intensities between the easy and stubborn switchers, we integrate radially, a narrow band containing the entire (200) ring (0.205 ± 0.004 nm), and calculate the standard deviation, σ, of the intensities along 2θ. From the measurements of 25 stubborn and 36 easy switchers, we found $1\sigma = 0.035 \pm 0.009$ and 0.063 ± 0.023 respectively, meaning, deviations from the average intensity along the (200) rings of the easy switchers are greater than those of the stubborn switchers. Aside from the (200) reflections, no other discrepancies were observed between those diffraction patterns of the easy and stubborn switchers.

We acquired dark-field images (fig. 3c) with the easy switchers' (200) spots, in order to visualize these grains. However, the smallest available objective aperture (5 μm diameter) on our microscope intersected not only the (200) spot, but also a portion of at least one neighboring ring. Therefore, we combine two separate images to form the (200) dark-field image. We acquired the first image by placing the objective aperture off-center around the (200) spot, avoiding the high-intensity (111) ring. When the objective aperture is placed this way, it intersects also, a part of (220) ring; all intensities within th e aperture contribute to the resulting dark-field image. The second image was acquired by shifting the aperture radially outward towards higher spatial frequencies, such that it simultaneously excludes the (200) spot and the (311) ring. Though not perfect, subtracting the second image from the first (fig. 3c) clearly shows the 200-diffracting, "trigger" grain. We call this the trigger grain for reasons soon to be explained.

Among the easy switchers, the locations of the (200) spots are random along 2θ, meaning, all trigger grains have [100] vectors lying randomly within the film plane. Sometimes two pairs of (200) spots are present with fourfold symmetry, suggesting that the [001] vector lies out of the film plane. A trigger grain may be found anywhere within a given dot and is usually between 10 to 14 nm in diameter or, twice the average grain size(7 nm). Fig. 3d is the bright-field image of the same dot in fig. 3b and c . The trigger grain is located at the circled region.

Based on the spacing measurements of the first four Debye rings, the Co/Pd appears to deviate slightly from the cubic form. Planar spacing ratios in cubic materials have specific relationships regardless of lattice parameter. For example, we expect the ratio of (200) and (220) spacings to be $\sqrt{2}$. For the Co/Pd multilayers, this ratio is slightly greater than $\sqrt{2}$ even after factoring in measurement uncertainties. Since Co and Pd have 9% lattice mismatch and that Co/Pd interface straining has been attributed as a source of perpendicular anisotropy[21,22], this is not an unexpected outcome. Additionally, ring broadening due to small grains adds to the uncertainty in the measurements.

Interactions between the separate dots are expected to be purely magnetostatic in origin. Interactions are approximated by the sum of dipole fields due to all the particles in the array, neglecting self-interactions, quadrapole, and higher order terms. For a perpendicularly magnetized array on a square grid with periodicity a, the dipolar field, H_{dipole}, is found numerically,

$$H_{\text{dipole}} = -0.7186\ M_s V/a^3 \approx -2.9kA/m. \qquad (1)$$

where the prefactor, 0.7186, was numerically calculated for variously sized arrays and extrapolated to an array of infinite size, M_s of Co is 1.8 T, $V = \pi r^2 t$, r is the dot radius and t is the Co thickness. Because this value is <1% of the difference between the measurement fields for the easy and stubborn switchers, dipolar interaction has negligible effect on our measurements.

Easy switchers have strong, discrete, (200) reflections while stubborn switchers do not. The strong reflections are caused by larger-than-average trigger grains with in-plane [100] vectors. It was previously proposed[19] that Co/Pd nanodots switch by rotation, that nevertheless, require the nucleation of Stoner-Wohlfarth (S-W) volumes. The size of the trigger grains in our easy switchers are on the same order as the estimated nucleation volume from ref. [17]. Furthermore, single crystal measurements on Co/Pd superlattices[23] showed that out-of-plane uniaxial anisotropy decreases (or even vanishes) as the surface normal vector changes from [111] to [110] and to [100]. With [100] vectors in-plane, the [111] is excluded from pointing out-of-plane. From the point of view of a nanodot, a larger-than-average grain with lower-than-average perpendicular anisotropy is effectively the weakest link, acting as the trigger center of each reversal event. In contrast, the stubborn switchers have fewer and smaller (200) grains, far smaller in volume compared with the typical trigger grain in an easy switcher. We therefore say that the stubborn switchers lack the trigger grain. Nandots of intermediate switching fields have varying degrees of (200) intensities and scatter along the (200) ring, indicating varying quantity and size of the trigger centers.

We found an important microstructural origin of SFD in Co/Pd nanodot arrays. Since grains with in-plane [100] vectors are correlated to dots with small switching fields, we conclude that these grains are the initial nucleation sites for the reversed domains. Furthermore, the degree of switching field suppression is linked to the size

of these trigger grains. The extent to which the [001] vector points out of plane may also play a role in reducing the switching field. Controlling the microstructure to eliminate the trigger grain may be the key to reducing the SFD Co/Pd nanodot arrays.

Acknowledgments

This work has been supported in part by the NIST-CNST/UMD-NanoCenter coop agreement, the NSF, and the NIH.

---

* Electronic address: june.lau@nist.govs

[1] C. Ross, Annu. Rev. Mat. Res. **31**, 203 (2001).
[2] M. Albrecht, C. T. Rettner, A. Moser, M. E. Best, and B. D. Terris, Appl. Phys. Lett. **81**, 2875 (2002).
[3] R. Dittrich, T. Schrefl, D. Suess, W. Scholz, and J. Fidler, IEEE Trans. Magn. **40**, 2507 (2004).
[4] B. D. Terris and T. Thomson, J. Phys. D **38**, R199 (2005).
[5] H. J. Richter, A. Y. Dobin, R. T. Lynch, D. Weller, R. M. Brockie, O. Heinonen, K. Z. Gao, J. Xue, R. J. M. van der Veerdonk, P. Asselin, M. F. Erden, et al., Appl. Phys. Lett. **88**, 222512 (2006).
[6] P. F. Carcia, J. Vac. Sci. Technol. A **5**, 1975 (1987).
[7] S. Hashimoto, Y. Ochiai, and K. Aso, J. Appl. Phys. **66**, 4909 (1989).
[8] W. B. Zeper, H. W. Vankesteren, B. A. J. Jacobs, J. H. M. Spruit, and P. F. Carcia, J. Appl. Phys. **70**, 2264 (1991).
[9] A. G. Roy, D. E. Laughlin, T. J. Klemmer, K. Howard, S. Khizroev, and D. Litvinov, J. Appl. Phys. **89**, 7531 (2001).
[10] R. Dittrich, T. Schrefl, A. Thiaville, J. Miltat, V. Tsiantos, and J. Fidler, J. Magn. Magn. Mater. **272-76**, 747 (2004).
[11] J. W. Lau, J. K. Bording, M. Beleggia, and Y. Zhu, Appl. Phys. Lett. **88**, 012508 (2006).
[12] J. Gadbois and J. G. Zhu, IEEE Trans. Magn. **31**, 3802 (1995).
[13] J. W. Lau, R. McMichael, M. A. Schofield, and Y. Zhu, J. Appl. Phys. **102**, 023916 (2007).
[14] M. Yoshikawa, E. Kitagawa, S. Takahashi, T. Kai, M. Amano, N. Shimomura, T. Kishi, S. Ikegawa, Y. Asao, H. Yoda, et al., J. Appl. Phys. **99**, 08R702 (2006).
[15] V. Parekh, E. Chunsheng, D. Smith, A. Ruiz, J. C. Wolfe, P. Ruchhoeft, E. Svedberg, S. Khizroev, and D. Litvinov, Nanotechnology **17**, 2079 (2006).
[16] J. M. Shaw, W. H. Rippard, S. E. Russek, T. Reith, and C. M. Falco, J. Appl. Phys. **101**, 023909 (2007).
[17] K. J. Kirk, J. N. Chapman, S. McVitie, P. R. Aitchison, and C. D. W. Wilkinson, J. Appl. Phys. **87**, 5105 (2000).
[18] O. Hellwig, A. Berger, T. Thomson, E. Dobisz, Z. Z. Bandic, H. Yang, D. S. Kercher, and E. E. Fullerton, Appl. Phys. Lett. **90**,162516 (2007).
[19] T. Thomson, G. Hu, and B. D. Terris, Phys. Rev. Lett. **96** 257204 (2006).
[20] V. Hou, Tech. Rep., Micron Technology, Inc. (2006).
[21] C. Chappert and P. Bruno, J. Appl. Phys. **64**, 5736 (1998).
[22] S. K. Kim and S. S.C., J. Appl. Phys. **89**, 3055 (2001).
[23] B. N. Engel, C. D. England, R. A. Vanleeuwen, M. H. Wiedmann, and C. M. Falco, Phys. Rev. Lett. **67**, 1910 (1991).